15TH IEA HEAT PUMP CONFERENCE
MAY 26–29, 2026 | HOFBURG
VIENNA 2026
DECARBONISATION THROUGH INNOVATION

Multi-stage water vapor high-temperature heat pump with latent thermal storage for extending temperature range

Seon Tae Kim*, Steffen Klöppel, Panagiotis Stathopoulos

Weinbergstr. 10, Cottbus, 03050, Germany

Abstract

An advanced multi-stage high-temperature heat pump (HTHP) was developed by adding two compression stages to an existing three-stage system, increasing the supply temperature from approximately 200 °C to 250 °C and extending its applicability for the effective electrification of industrial process heat. In addition, two latent thermal energy storage (LTES) units, one for each temperature level, were integrated to mitigate mismatches between heat supply and demand, which are expected to become more pronounced as the share of renewable energy increases, by providing peak-shaving capability. The HTHP coupled by split valves between the existing three stage compression cycle and an additional two stage cycle achieved a COP of 2.4−3.2 depending on the split ratio and consistently delivered over 1 MW of total heat output under the rated temperature conditions. When the HTHP operated under various temperature conditions, while maintaining identical temperature lifts between the existing and additional compression stages, both total heat output and compressor power consumption increased as the temperature level dropped. The required heat storage capacities of the LTES systems were estimated assuming each unit stores sufficient heat for up to 6 hours of peak-shaving operating at nominal HTHP conditions. Increasing split ratio reduces storage needed for the lower-temperature LTES, around 200 °C, but raises it for the higher temperature, around 250 °C. In particular, even when all main flow goes to the additional compression stages, the lower-temperature LTES must can store certain amount energy because the existing HTHP cycle requires heat-sink flow to limit superheat between its compression stages. The integrated system, comprising the advanced multi-stage HTHP and dual LTES configuration, is expected to improve the feasibility of industrial heat electrification and provide demand-side flexibility by supplying heat with higher efficiency and enabling effective peak-shaving.

Keywords: High-Temperature Heat Pump; R-718 (water);Multi-stage vapor compression cycle; Latent Thermal Energy Storage;

1. Introduction

The continued rise in global greenhouse gas (GHG) emissions over recent decades remains a critical challenge in addressing climate change. Carbon dioxide (CO_2), the primary contributor to global warming, is predominantly emitted through the combustion of fossil fuels. The industrial sector accounts for approximately 37% of total global energy consumption, with nearly two-thirds of this energy allocated to heat generation [1-2]. Consequently, industrial heat demand constitutes over 20% of global energy consumption, underscoring the necessity of decarbonization strategies within this sector. Electrification of industrial process heat has been identified as one of the most effective strategies for achieving substantial reductions in CO_2 emissions. Industrial heat provision technologies can be broadly classified into two categories: boilers, which supply heat at low and medium temperatures, typically up to 500 °C, and process heaters or furnaces, which operate at higher temperatures. While high-temperature heat, above 500 °C, is generated either directly or indirectly through process heaters or furnaces, low- to mid-temperature heat is predominantly supplied by gas-fired boilers. Given the significant share of energy consumption associated with this temperature range, the

* Corresponding author. Tel.: +49-3583-58545-14
E-mail address: seon.kim@dlr.de

electrification of low- and mid-temperature industrial heat presents a substantial opportunity for CO_2 emission mitigation within industrial processes [3-4].

The electrification of industrial process heat using renewable electricity is considered an effective approach to mitigating CO_2 emissions from industry. Natural gas boilers, which mainly used to supply industrial process heat, have emission factor of approximately 235 g_{CO2eq}/kWh, whereas renewable electricity generally emits less than 50 g_{CO2eq}/kWh [5-6]. Considering that the current electricity generation emission factor at the European Union level is 187.08 g_{CO2eq}/kWh in 2024 and is expected to fall below 120 g_{CO2eq}/kWh by 2030, it is essential to increase the share of renewable energy sources with near-zero CO_2 emission [7]. Furthermore, technology capable of efficiently utilizing this growing share of renewable energy will be required.

There is a wide range of mature electrification technologies that can convert electric power to heat, currently available to meet industrial heat demand across various temperature ranges and applications. In particular, heat pump technology, which is capable of supplying heat up to approximately 150 °C, is expected to play an important role not only in the electrification of industrial processes but also in enhancing the overall efficiency of process due to its high coefficient of performance (COP) [8].

In current study, the integrated system of an industrial high-temperature heat pump (HTHP) and latent thermal energy storage (LTES) is investigated to facilitate a successful energy transition based on renewable electricity. The multistage water vapor compression HTHP, which is being developed by author's research group, is expected to supply at around 200 °C, with plans to add additional compression stages to raise the temperature level up to 250 °C [9]. This HTHP, which uses a natural refrigerant water/steam, is expected to effectively mitigate CO_2 emissions due to low global warming potential (GWP) of the refrigerant. Among the various energy storage technologies, thermal energy storage (TES) is regarded as the most promising storage method for the HTHP system. Particularly, the LTES system has a higher energy density than conventional sensible TES systems and has already reached high technical readiness levels (TRL) [10]. This LTES technology is expected to enhance the overall operation efficiency by overcoming the inherent limitation of the mismatch between unstable electricity supply from renewable energy and the fluctuation of industrial demands [11]. In particular, the integrated system can reduce high-energy demand period by first storing thermal energy generated by the heat pump during off-peak, low-cost hours subsequently utilizing this stored energy during peak periods. Therefore, this study investigates not only the overall thermodynamic performance of the developing multistage water vapor compression HTHP, but also the appropriate LTES materials and the corresponding required quantities under various operating conditions to enable effective industrial peak shaving.

2. System modeling

The schematic diagram of integrated system, comprising the HTHP and LTES, is shown in Fig. 1. The additional two compression stages, brown dotted line, were introduced into the existing HTHP system, which already includes three compression stages, to enhance the supply heat temperature from around 200 °C up to approximately 250 °C. All compression stages, both existing and additional, employ turbo compressors suitable for large capacity application. The advanced HTHP cycle, comprising the existing and additional stages, features two heat sink outlets, one from the existing HTHP and the other from the additional HTHP, to meet the requirements of two different temperature levels for distinct industrial processes. Furthermore, two distinct LTES systems were designed to store and supply thermal energy for each temperature level, utilizing different phase change materials (PCM) to address the mismatch in demand response.

The proposed HTHP cycles were modeled with EBSILON Professional 17 using IAPW-IF97 as the standard thermodynamic fluid library of water steam. There are three temperature variables for the advanced HTHP system. The evaporation temperature, T_{Evap}, corresponding to state points 1–2 in Fig. 1, was varied between 90 and 110 °C. The condensation temperatures for the existing HTHP, $T_{Cond\text{-}HTHP1}$ (state points 3–4), and the additional compression stages, $T_{Cond\text{-}HTHP2}$ (state points 5–6), were assumed to be in the range of 190–210 °C and 240–260 °C, respectively. Additionally, the degrees of subcooling and superheating were both set to 10 K, T_{Sub} & T_{Sup} = 10 K. The mass flow rate of the existing main cycle, $\dot{m}_{main}$, is 0.4 kg/s, and the split ratio, $\beta = \dot{m}_{split}/\dot{m}_{main}$, for the additional compression stage was varied from 0 to 1. In practical industrial processes, the required heat demand at each temperature level varies over time. Accordingly, the heat supply to each temperature level can be flexibly controlled by adjusting the split ratio to match the time-dependent demand. The isentropic and mechanical efficiencies of the compressors, η_s and η_m, were assumed to be 0.70 and 0.99, respectively. Particularly, each compressor was assigned the same pressure ratio for the existing HTHP and the additional stages, respectively, according to boundary conditions, as previous studies have shown that multistage heat pump cycles achieve the highest COP under this condition [9]. The pressure levels of the sink flows passing though the intercoolers and condensers were set to be 1.0 bar below the respective condenser pressure of both the HTHP cycle and the additional stages. Furthermore, the heat sink flow rates were adjusted to maintain a temperature difference of 10 K between the outlet of the intercooler and the inlet of the condensers. This adjustment prevents pinch point violations in the heat exchangers and ensures complete heat recovery.

Two distinct LTES systems, intended to balance temporal mismatches between heat supply and demand, are connected to the heat sink flows of the HTHP system. Different eutectic compositions of inorganic salts are introduced for each temperature level: a magnesium nitrate ($Mg(NO_3)_2$) and sodium nitrate ($NaNO_3$) mixture for the existing HTHP system (LTES 1), and a sodium nitrate ($NaNO_3$) and potassium nitrate (KNO_3) mixture for the 250 °C system (LTES 2). The eutectic compositions for LTES1 consist of 0.48 and 0.52 mole fraction of $Mg(NO_3)_2$ and $NaNO_3$, respectively, resulting in a melting point, T_m, of approximately 177 °C with 119 kJ/kg of enthalpy of fusion, H_f [12]. For the LTES2, a mixing mole ratio of 0.51 KNO_3 and 0.49 $NaNO_3$ was used, resulting in a T_m of approximately 222 °C with 108 kJ/kg of H_f [13]. The operating strategies of the LTES systems can be categorized into storage, discharge, and standby modes. The amount of heat stored in each LTES system can be controlled via the split ratio, and the store heat is discharged through separate heat sink flow. In practice, an LTES system cannot achieve complete storage and discharge of thermal energy due to thermal losses and operation constrains. However, in this study, a simplified system-level assumption of complete storage of the heat transferred from the heat sink fluid is adopted in order to estimate the required amount of PCM.

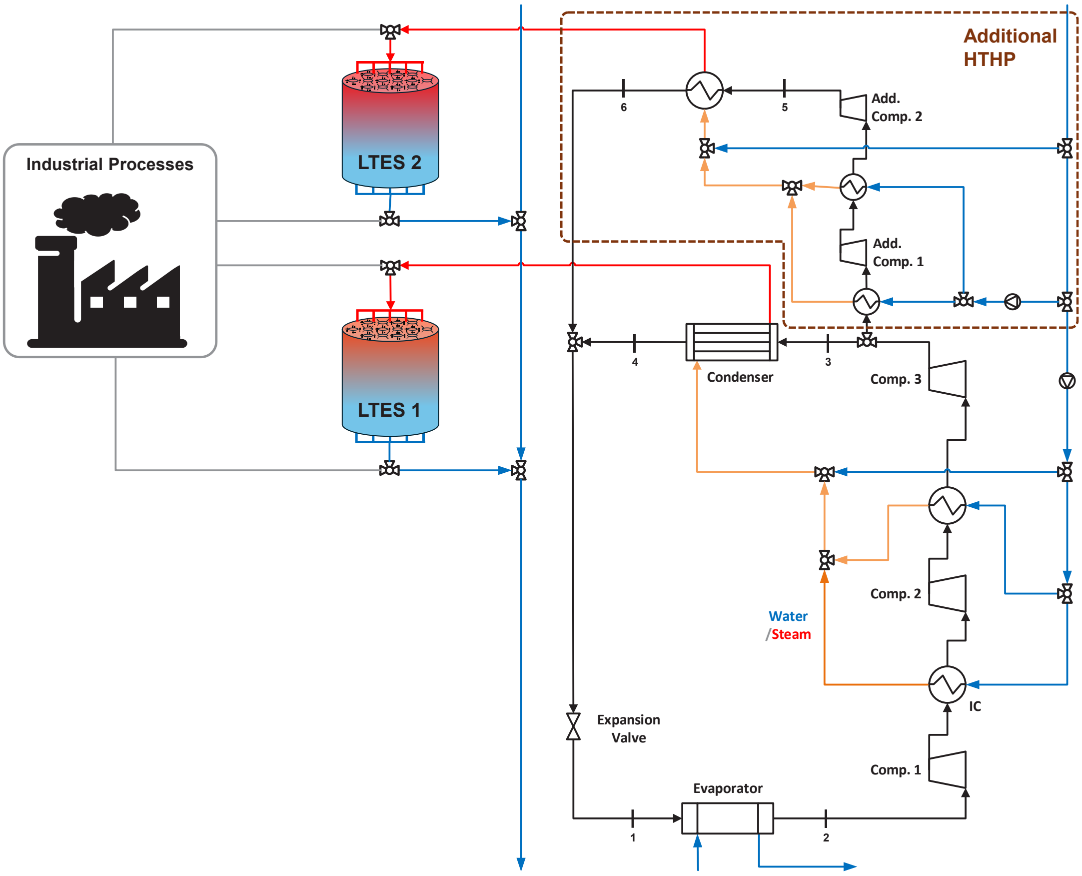

Figure 1. Schematic diagram of the integrated multistage HTHP-LTES system in heat storage mode.

3. Performance analysis

3.1. Multistage HTHP performance

The thermodynamic performance of the proposed multistage HTHP cycle was evaluated from the perspectives of the heat sink flow, since the useful heat available for industrial processes originates from the heat sink rather than from the main cycle flow, Q_{HTHP1} and Q_{HTHP2}. The coefficient of performance (COP) was defined as the ratio of the total useful heat output, $Q_{\text{total}} = Q_{\text{HTHP1}} + Q_{\text{HTHP2}}$, to the total compressor power consumption, W_{comp}, Eq (1).

$$\text{COP} = \frac{Q_{total}}{W_{\text{comp}}} = \frac{Q_{\text{HTHP1}} + Q_{\text{HTHP2}}}{W_{\text{comp}}} \tag{1}$$

A comparison of the thermodynamic performance of the proposed multistage HTHP under three different temperature conditions, each characterized by the same temperature lifts, 100 K for $T_{\text{Cond-HTHP1}}$ and 50 K for $T_{\text{Cond.-HTHP2}}$, is presented in Fig. 2. Although the values of ΔT_{lift} are the identical, the cycle operating at lower T_{Evap}, $T_{\text{Cond-HTHP1}}$, and $T_{\text{Cond-HTHP2}}$ exhibits a higher total useful heat output, Q_{total}. This enhancement can be attributed to the increased mass flow rate of the heat sink through the intercoolers and condensers in the HTHP cycle. Under the boundary conditions considered in this study, the compressor inlet condition is assumed to be 10 K superheated, therefore, the required refrigerant-side heat removal in the heat exchangers increases with the degree of superheat. Since the discharge temperature after compressor can be estimated from Eq. (2), the required heat removal and corresponding heat sink flow rate can also be calculated. In particular, it was found that cycles with lower evaporation temperatures exhibit a higher degree of superheating, even though all simulations were conducted with the same overall temperature lifts and equal pressure ratios for each compression stage. This is because the stage pressure ratios, $P_{\text{dis}}/P_{\text{in}}$ in Eq. (2), increase as the evaporation temperature decreases. As a result, higher pressure ratio at lower evaporation temperatures lead to a higher degree of superheating and, consequently, a higher heat sink mass flow rate is required to cool the refrigerant to the designed superheat level, $T_{\text{Sup.}} = 10$ K.

$$T_{\text{dis}} = T_{\text{in}} + \frac{T_{\text{in}}}{\eta_{\text{s}}}\left(\left(\frac{P_{\text{dis}}}{P_{\text{in}}}\right)^{\left(\frac{\kappa-1}{\kappa}\right)} - 1\right) \tag{2}$$

where T_{in} is inlet temperature, T_{dis} is the discharge temperature, P_{in} is the inlet pressure, P_{dis} is the discharge pressure, κ is the specific heat ratio, and η_{s} is the isentropic efficiency.

The HTHP cycle operating under the highest temperature conditions ($T_{\text{Evap.}} = 110$ °C, $T_{\text{Cond-HTHP1}} = 210$ °C, $T_{\text{Cond-HTHP2}} = 260$ °C) exhibits a 4.6% lower total heat output, Q_{total}, than that under the lowest temperature conditions ($T_{\text{Evap.}} = 90$ °C, $T_{\text{Cond-HTHP1}} = 190$ °C, $T_{\text{Cond-HTHP2}} = 240$ °C) when the split ratio is zero, corresponding to operation of only the existing HTHP. This discrepancy increases to 5.5% when the split ratio is one, corresponding to operation of only the additional HTHP. In particular, when the total heat output, Q_{total}, is divided into Q_{HTHP1} and Q_{HTHP2}, Q_{HTHP2} under the highest temperature conditions is consistently 5.1% lower than that under the lowest temperature conditions. In contrast, the difference in Q_{HTHP1} increases from 4.6% to 7.8% as the split ratio increase. In terms of compressor power consumption, W_{comp}, the HTHP operating under the lowest temperature conditions exhibits higher power consumption than under the highest temperature conditions, due to the higher-pressure ratio explained above.

The coefficient of performance of the HTHP decreases with increasing split ratio under all temperature conditions, as the compressor power, W_{comp}, increases with split ratio, while the total useful heat Q_{total} remains nearly constant. This is due to the increased mass flow rate toward the higher condensation temperature. Although the HTHP operating under the lowest temperature conditions ($T_{\text{Evap.}} = 90$ °C, $T_{\text{Cond.-HTHP1}} = 190$ °C, $T_{\text{Cond.-HTHP2}} = 240$ °C) has 2.3-5.5% higher Q_{total}, it also requires 4.1-8.0% higher W_{comp}. Consequently, the HTHP cycle operating under the highest temperature conditions ($T_{\text{Evap.}} = 110$ °C, $T_{\text{Cond.-HTHP1}} = 210$ °C, $T_{\text{Cond.-HTHP2}} = 260$ °C) achieves a higher COP than the other operating conditions at the same split ratio.

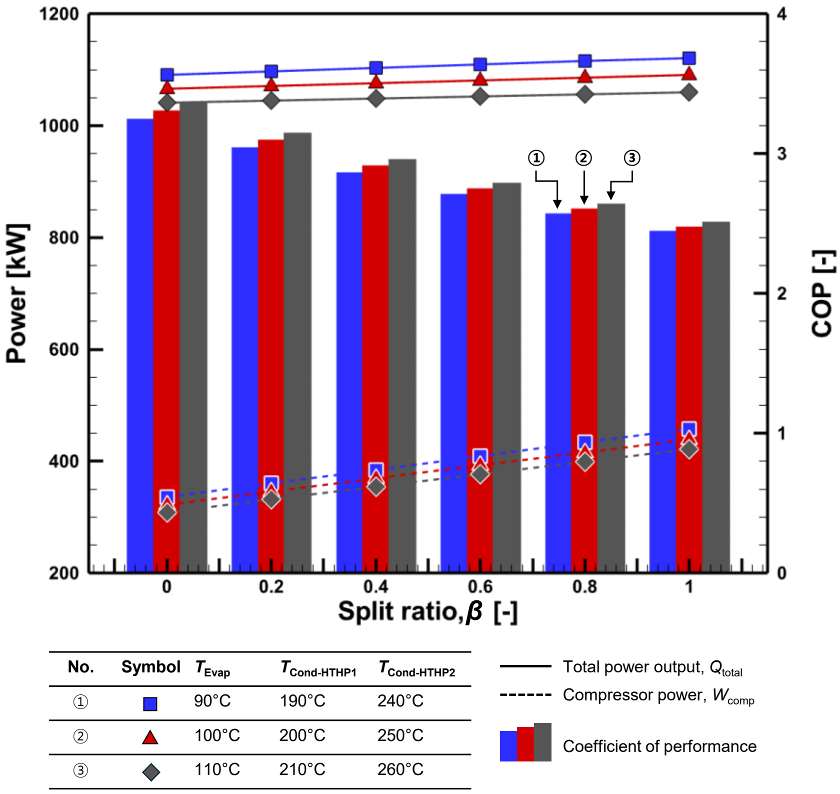

Figure 2. Thermodynamic performance of the HTHP cycle, heat output rate and COP, under the same temperature lifts.

3.2. Required LTES capacity

The respective useful heat outputs, Q_{HTHP1} and Q_{HTHP2}, and the required PCM quantities for the LTES systems were evaluated. Since peak-shaving applications in industrial processes typically require several hours of operation or discharge, the heat supplied to each LTES system was estimated for up to 6 hours steam-demand scenarios under the nominal HTHP operating conditions (T_{evap} = 100 °C, $T_{cond\text{-}HTHP1}$ = 100 °C, $T_{cond\text{-}HTHP2}$ = 250 °C). As shown in Fig. 3, the heat output rates of Q_{HTHP1} decreases with increasing split ratio, whereas Q_{HTHP2} increases. Moreover, Q_{HTHP2} exceeds Q_{HTHP1} when the split ratio reaches 0.6 rather than 0.5, even though the mass flow rate directed to the additional HTHP becomes higher. This behavior arises because the existing HTHP cycle includes one more intercooler than the additional HTHP cycle, which contributes additional heat output. Consequently, operation for up to 6 hours under nominal conditions requires approximately 23,024 MJ of stored heat for LTES1 at β = 0, corresponding to 193.48 tonnes of PCM1, and approximately 20,028 MJ for LTES2 at β = 1, corresponding to 185.44 tonnes of PCM2. Notably, LTES1 requires at least 29.60 tonnes of PCM1, even when all refrigerant is directed to the additional HTHP cycle, to store 3,522 MJ of heat generated during cooling of the superheated vapor after the compression stages of the existing HTHP system. In contrast, PCM2 is not required when the additional HTHP is not in operation, β = 0.

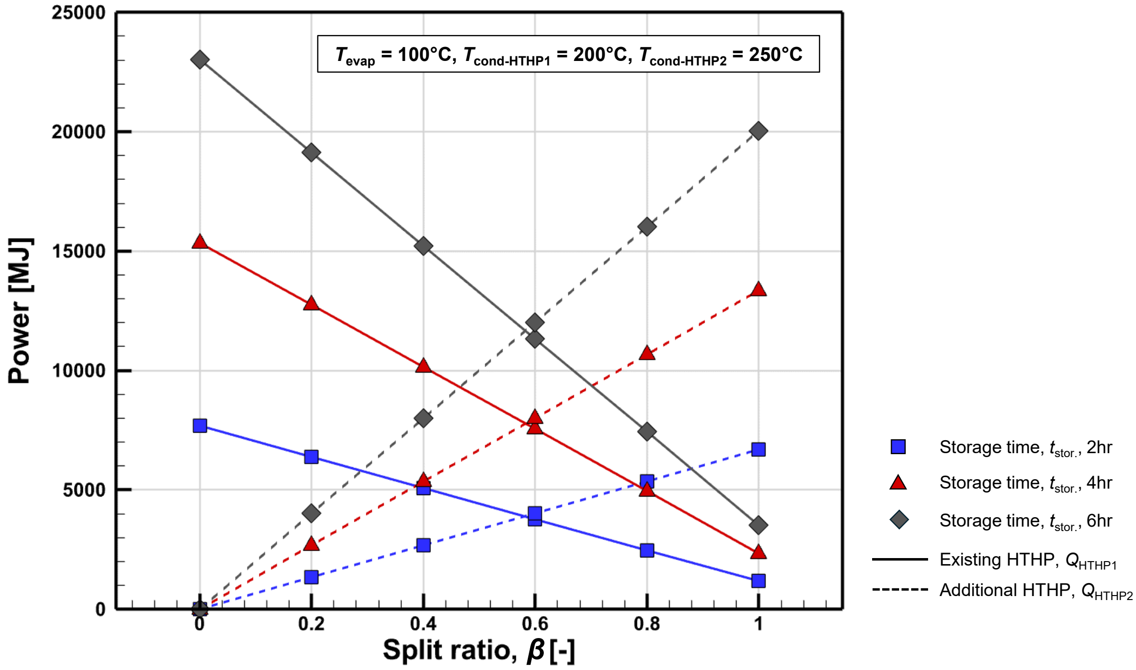

Figure 3. Heat output rates Q_{HTHP1} and Q_{HTHP2} as a function of for steam demand periods of 2, 4, and 6 hours.

4. Conclusions

The additional two compression stages were incorporated into the existing three stage HTHP system to increase the heat supply temperature from approximately 200 °C to about 250 °C. In addition, two separated LTES systems were introduced for each temperature level to address the mismatch between supply and demand and to enable effective peak shaving.

Although the total heat output rate is not affected largely by changes in split ratio, the compressor power consumption increases due to the higher mass flow rate of the main cycle directed toward the higher-temperature stages. Although the HTHP cycle have the same temperature lifts, the cycle operating under lower temperature conditions exhibits higher compressor power consumption and total heat output. This is attributed to the higher-pressure ratios for each compression stage and the increased heat sink flow rate needed to effectively reduce higher degree of superheating. The useful heat output rates from the two heat sink flows over 6 hours, as well as the corresponding amounts of required PCMs, were estimated under the assumption that the LTES system operate for peak-shaving. As expected Q_{HTHP1} decreases and Q_{HTHP2} increases with the split ratio, with the two values intersecting at a split ratio of approximately 0.6. Notably, LTES1 still requires at least 3,522 MJ of stored heat, 29.60 tonnes of PCM2, even when the entire main flow is directed to the additional cycle, because the existing HTHP cycle continues to require a minimum heat sink flow to cool the main stream between compression stages.

Although both the HTHP and LTES systems considered in this study are scalable, the limited operating conditions may lead to an optimistic estimation of system performance. Therefore, further investigations of the thermodynamic performance of the integrated HTHP and LTES system under various conditions, such as operating temperature, split ratio, and operating strategies, will be conducted to better characterize the system and understand the interactions among these variables. Nevertheless, the present results provide useful insights into the potential of the integrated system for effective CO_2 mitigation in industrial processes through an effective energy transition.

Acknowledgements

This research was funded by CETPartnership, the Clean Energy Transition Partnership under the 2023 joint call for research proposals, co-funded by the European Commission (GA N°101069750) and with the funding organizations detailed on https://cetpartnership.eu/funding-agencies-and-call-modules.

References

[1] International Energy Agency (IEA). *World Energy Outlook 2021*. Paris: IEA; 2021.
[2] International Energy Agency (IEA). *Clean and efficient heat for industry*. Paris: IEA; 2018.
[3] Marina A, Spoelstra S, Zondag HA, Wemmers AK. An estimation of the European industrial heat pump market potential. *Renew. Sustain. Energy Rev.* 2021; **139**: 110545.
[4] Matthias R, Tobias F, Felipe T. A bottom-up estimation of the heating and cooling demand in European industry. *Energy Efficiency* 2017; **11**: 1057–82.
[5] Alesandro C, Pietro C, Fulvio S, Rajandrea S. Environmental and economic benefits from the phase-out of residential oil heating: A study from the aosta valley region. *sustainability* 2019;**11**:3633.
[6] Nana YA, Mads T, Bethany K, Inge A, Rupert LH. Greenhouse gas emissions from renewable energy sources: A review of lifecycle consideraitons. *Renew. Sustain. Energy Rev.* 2014;**39**:461-475.
[7] European Environment Agency (EEA). 2025. Greenhouse gas emission intensity of electricity generation in Europe, European Environment Agency (accessed 16 November 2025)
[8] Cordin A, Frédéric B, Michael U, Jürg S, Stefan SB. High temperature heat pumps: Market overview, state of the art, research status, refrigerants, and application potentials. *Energy* 2018;**152**:985-1010.
[9] Seon Tae K, Robert H, Göksel Ö, Panagiotis S, Eberhard N. Performance analysis of multistage high-temperature heat pump cycle. *Energy Sci. Eng.* 2023;**11**:3500-11.
[10] Tian Y, Zhao CY. A review of solar collectors and thermal energy storage in solar thermal applications. *Appl. Energy* 2013;**104**:538-53.
[11] Miró L, Gasia J, Cabeza LF. Thermal Energy Storage (TES) for Industrial Waste Heat (IWH) Recovery: A Review. *Appl. Energy* 2016;**179**:284-301.
[12] Yuan Z, Junsheng Y, Min W, Jinli L. Phase diagrams of binary systems $Mg(NO_3)_2$-KNO_3, $Mg(NO_3)_2$-$LiNO_3$ and ternary system $Mg(NO_3)_2$-$LiNO_3$-$NaNO_3$. *J. Chem. Eng. Data* 2020;**65**:3420-7.
[13] Thomas B, Doerte L, Rainer T. Overview of PCMs for concentrated solar power in the temperature range 200 to 350 °C. *Adv. Sci. Technol.* 2010;**74**:272-7.